First Preclinical Imaging of Primary Cartilage Neoplasm and Its Local Recurrence Using ^{99m}Tc-NTP 15-5 Radiotracer

Elisabeth Miot-Noirault[1], François Gouin[2], Aurélien Vidal[1], Maryse Rapp[1], Jean Maublant[1], Serge Askienazy[3], Jean-Michel Chezal[1], Dominique Heymann[2], Françoise Redini[2], and Nicole Moins[1]

[1]EA 4231, Université d'Auvergne, INSERM UMR 484, and Centre Jean Perrin, Clermont-Ferrand, France; [2]INSERM UMR S957 EA3822, Université de Nantes, Nantes, France; and [3]Cyclopharma Laboratoires, Saint Beauzire, France

This study on a rat model of grade II chondrosarcoma aimed to determine whether the radiotracer *N*-(triethylammonium)-3-propyl-[15]ane-N5 radiolabeled with ^{99m}Tc (^{99m}Tc-NTP 15-5), which binds to cartilage proteoglycans, has pathophysiologic validity for in vivo imaging of cartilage tumoral tissue. **Methods:** We used 2 experimental approaches with the Swarm chondrosarcoma rat model: that is, a primary paratibial location and local recurrence after intralesional curettage. ^{99m}Tc-NTP 15-5 scintigraphy and ^{99m}Tc-hydroxymethylenediphosphonate (^{99m}Tc-HMDP) scanning were performed at regular intervals during 50 d after tumor implantation in a paratibial location (primary model; $n = 12$ animals) and after intralesional curettage in a femoral condyle location (recurrence model; $n = 9$ animals). For each animal, positive scans were analyzed at each time point using the target-to-background ratio (TBR), with the target region of interest delineated over the tumor and the background region of interest over muscle. In each model, the TBR time course was followed against primary tumoral growth or recurrence. Tumor volume was monitored for 2 mo by measuring the 2 perpendicular diameters. At study end, animals were sacrificed for histopathologic analysis. **Results:** For both models, ^{99m}Tc-NTP 15-5 scans showed tracer accumulation at the site of implantation or curettage. For the primary tumor model, the mean TBR was 1.6 ± 0.14 by day 4 after implantation and increased over time as the disease progressed, with a mean TBR of 4.25 ± 0.25 on day 45. For the recurrence model, mean TBR was 3.27 ± 0.24 by day 4 after curettage and increased with recurrence, with a mean value of 5.25 ± 0.49 on day 50. ^{99m}Tc-HMDP bone scans were negative for both models throughout the study; at a later stage of the study, an area of ^{99m}Tc-HMDP accumulation was seen in the diaphysis of the bone adjacent to the tumor and was attributed to remodeling. **Conclusion:** These experimental results in 2 preclinical models of grade II chondrosarcoma bring forward data in favor of ^{99m}Tc-NTP 15-5 radiotracer for imaging primary growth of chondrosarcoma and its local recurrence after surgery.

Key Words: proteoglycans; chondrosarcoma; scintigraphy; ^{99m}Tc-NTP 15-5 radiotracer

J Nucl Med 2009; 50:1541–1547
DOI: 10.2967/jnumed.108.056721

Received Aug. 8, 2008; revision accepted Jan. 9, 2009.
For correspondence or reprints contact: Elisabeth Miot-Noirault, EA 4231, INSERM UMR 484, rue Montalembert, BP 184, 63005 Clermont-Ferrand, France.
E-mail: elisabeth.noirault@inserm.fr

Chondrosarcomas are a heterogeneous group of slow-growing, malignant bone tumors that have in common the production of a hyaline cartilagelike extracellular matrix (*1*). Chondrosarcoma is the second most common type of skeletal malignancy, with a survival rate at 10 y ranging from 46% to 70% depending on the series (*2–4*). To orthopedic oncologists, cartilage tumors still present a challenge in diagnosis and therapy (*3–6*). Evaluation of the disease combines clinical picture, radiography, CT, MRI, and the 3-level histopathologic grading of Evans (*7–10*). The Evans classification is based on cell type, cell differentiation, matrix formation, and architecture and is considered useful for the prediction of clinical behavior (*6,9–14*). To date, many questions remain unanswered, and there is an urgent need for markers that characterize biologic phenotypic features of the tumor to guide clinical decision making (*6,8,15,16*).

The proteoglycan matrix of chondrosarcomas is composed mainly of aggrecan-type proteoglycans (*1,13,14*). Aggrecan is a complex macromolecule made up of a central core protein to which numerous chondroitin sulfate and keratan sulfate glycosaminoglycan chains are covalently bound. Because of the high sulfate and carboxyl group content of their glycosaminoglycan moieties, proteoglycans of extracellular matrix have strong negative charges that have been shown (by our group and others) to interact with the positively charged quaternary ammonium function (*17,18*).

These observations led our group to develop a cartilage targeting strategy that uses the quaternary ammonium function as a carrier to deliver therapeutic drugs or radioactive isotopes selectively to cartilage tissue (*19*). The strategy for application to cartilage imaging is based on the use of bifunctional agents containing a quaternary ammonium function able to bind to cartilage proteoglycan and a polyazamacrocycle structure able to complex ^{99m}Tc (*20*). For this purpose, *N*-(triethylammonium)-3-propyl-[15]ane-N5 radiolabeled with ^{99m}Tc (^{99m}Tc-NTP 15-5) was selected in view of the high stability of the ^{99m}Tc-complex and its

high in vitro and in vivo affinity for proteoglycan (*21,22*). The high accumulation and specific localization properties of ^{99m}Tc-NTP 15-5 in cartilage, together with high target-to-nontarget ratios, should allow high-contrast SPECT of articular function (*22,23*).

Because chondrogenic tumors are characterized by the presence of hyaline cartilagelike extracellular matrix, we hypothesized that the ^{99m}Tc-NTP 15-5 tracer could be useful for the scintigraphic detection of chondrosarcoma. The relevance of ^{99m}Tc-NTP 15-5 imaging for the diagnosis of primary chondrosarcoma and its local recurrence was assessed in the Swarm rat chondrosarcoma (SRC) model, using 2 experimental approaches: primary paratibial tumor development, and local tumor recurrence after intralesional curettage (*24,25*). These first experimental results suggest that ^{99m}Tc-NTP 15-5 scintigraphy may be useful for the evaluation of the tumoral pathology of cartilage.

MATERIALS AND METHODS

Animals

Twenty-one male Sprague–Dawley rats (Charles River) were used for this study. They were handled and cared for in accordance with the *Guide for the Care and Use of Laboratory Animals* (*26*) and European directive 86/809/EEC. They were maintained at 21°C with a 12-h/12-h light/dark cycle. Protocols were performed under the authorization of the French Directorate of Veterinary Services (authorization C63-113-10) and were conducted under the supervision of authorized investigators in accordance with the institution's recommendations for the use of laboratory animals. The animals were randomly divided into 2 groups, with 12 animals being in the primary chondrosarcoma model and 9 in the tumor local recurrence protocol.

Anesthesia

For tumoral implantation and curettage, the rats were anesthetized by inhalation of isoflurane (Abbott) in air (1.5%, 1 L/min) in association with an intramuscular injection of 100 mg of ketamine (Imalgène; Rhone Merieux) per kilogram of body weight.

For scintigraphic acquisition, the animals were anesthetized with a mixture of ketamine (35 mg/kg intramuscularly) (Imalgène 500) and xylazine (5 mg/kg intramuscularly) (Rompun 2%; Bayer).

Tumor Models

The SRC line was a generous gift from Dr. Patrick A. Guerne (Geneva, Switzerland) as tissue fragments, which were frozen until use. The SRC model is a tumor tissue line derived from a tumor that arose spontaneously in the thoracic and lumbar vertebrae of a female Sprague–Dawley rat. The SRC tissue line has been maintained over the years by serial subcutaneous injections, and its histochemical characteristics have remained stable in successive transplants: it is a well-differentiated chondrosarcoma with mild cellular atypia (grade II) (*24,25*).

Tumor fragments were collected from well-developed tumors on the paratibial area of donor Sprague–Dawley rats. These fragments were immediately stored in cold α-minimum essential medium and manually calibrated to 10 mm^3. Allograft transplantation of a 10-mm^3 SRC fragment was performed on the right paw, the other paw being used as the contralateral reference (*24,25*).

Model of Primary Chondrosarcoma Induced by Unilateral Paratibial Implant. Using a lateral approach, the cortical surface of the diaphysis was scarified laterally over 10 mm, a 10-mm^3 SRC fragment was placed contiguous with the scarified surface, and the muscular and cutaneous wounds were sutured (*24,25*). The same procedure was performed for the contralateral paw, but no tumor fragment was implanted.

Model of Local Tumor Recurrence After Intralesional Curettage. Using a lateral approach facing the right femoral condyle, a 3-mm-diameter hole was drilled to access the medullary cavity, where an SRC fragment was implanted using a curet and the incision sutured. For the contralateral paw, a 3-mm-diameter hole was drilled, but no tumor fragment was implanted. When the tumors had reached a volume of approximately 1,200 mm^3 (considered progressive tumors), the animals underwent intralesional curettage (*24,25*).

Tumor Growth Assessment

Two perpendicular diameters were measured using a caliper, and tumor volume was estimated using the formula $V = 0.5 \times L \times S^2$, where L and S were, respectively, the largest and smallest perpendicular tumor diameters (*24*).

Radiolabeled Tracers

N-(triethylammonium)-3-propyl-[15]ane-N5 (NTP 15-5) was prepared and radiolabeled with ^{99m}Tc by the stannous chloride method as previously described, with a specific radioactivity of 25 MBq/μmol (Fig. 1) (*20*). Quality control was performed with Partisil KC18F strip thin-layer chromatography (Whatman), using methanol:acetonitrile:tetrahydrofuran:ammonium acetate (1N) (3:3:2:2) as eluent.

Bone scanning was performed using the ^{99m}Tc-hydroxymethylenediphosphonate (^{99m}Tc-HMDP) kit for human use (Osteocys; IBA).

For each radiotracer, the activity delivered to each animal was determined by measuring the activity of the syringe before and after injection, using a dose calibrator (Capintec).

Tolerance to repeated injection of both tracers over 2 mo was also evaluated as previously described (*23*).

γ-Camera

Scintigraphic in vivo imaging was performed using a small-animal γ-camera (CsI(Na) crystal) equipped with a 1.3/0.2/35 parallel-hole collimator (hole diameter/septum thickness/height in mm) (Gammaimager; Biospace). All acquisitions were performed with a 15% window centered on the 140-keV photopeak of ^{99m}Tc.

Sequential Imaging of Primary Chondrosarcoma and Recurrent Tumor Models with ^{99m}Tc-NTP 15-5 Tracer

Primary chondrosarcoma-bearing rats underwent 7 scintigraphic examinations on days 4, 7, 10, 20, 25, 35, and 45 after implantation. Animals in the recurrent tumor group underwent scintigraphic examinations on days 4, 10, 20, 30, 35, 40, and 50 after intralesional curettage.

Scintigraphic acquisition was performed 15 min after intravenous administration of 30 MBq of ^{99m}Tc-NTP 15-5, on the basis of previous studies showing that high-contrast cartilage images could be obtained from this delay (*21–23*). For both groups, a 10-min planar acquisition was performed for each posterior paw of animals positioned over the collimator of the camera.

^{99m}Tc-NTP 15-5 scans were considered positive when tracer uptake areas corresponded to sites of implantation or curettage. All the scans were evaluated by the same experienced investigator,

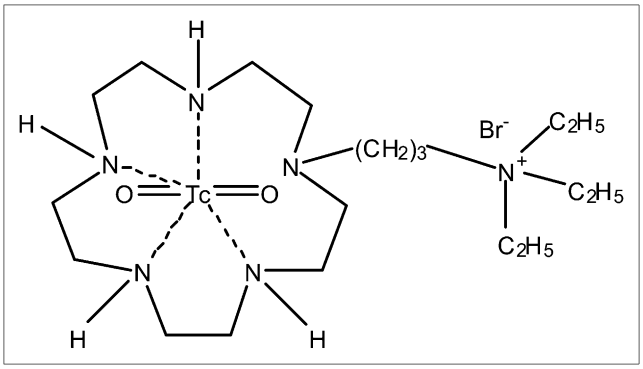

FIGURE 1. Chemical structure of ^{99m}Tc-*N*-[triethylammonium]-3-propyl-[15]ane-N5 (^{99m}Tc-NTP 15-5).

using fixed-size regions of interest (ROIs) delineated over tumor and muscle patterns. An ROI of equal size was also placed over the contralateral femorotibial cartilage pattern (Supplemental Fig. 1; supplemental materials are available online only at http://jnm.snmjournals.org). The use of an activity profile for ROI placement ensured easy, reproducible positioning of the ROI for serial images in the same animal over time and among all the animals imaged. For each ROI, total activity, average count in cpm per pixel, and activity SD were obtained.

At each time point and for each animal, target-to-background ratio (TBR) was calculated as follows:

TBR_T = average count in tumor/average count in muscle.

TBR_C = average count in contralateral femorotibial cartilage/average count in muscle.

At each time point, TBR parameters were averaged per group. Data were expressed as mean ± SD. For both models, 2 analyses were performed: First, the mean TBR_T determined on day 4 was used as the threshold reference value and was compared with the mean TBR_T determined at each time point of study (paired 2-sided Student *t* test with a level of significance set at $P < 0.05$). Second, at each time point, the mean TBR_T was compared with the mean TBR_C (ANOVA with a level of significance set at $P < 0.05$).

Dynamic Planar Imaging of ^{99m}Tc-NTP 15-5 Distribution in Rats with Well-Established Primary Chondrosarcoma

Dynamic planar imaging in list mode was performed on rats with primary tumors (mean volume, 949.35 ± 223 mm^3). The tumor-bearing paws of anesthetized animals (n = 5) were positioned over the collimator of the γ-camera. Rats then received an intravenous injection of 30 MBq of ^{99m}Tc-NTP 15-5 that was simultaneous with the start of a 90-min acquisition, being postprocessed with a 30-s sampling time. Time–activity curves were obtained from fixed ROIs drawn around the tumor, femorotibial joint, and muscle, with activities corrected for radioactive decay.

Sequential Imaging of Primary Chondrosarcoma and Recurrent Tumor Models with ^{99m}Tc-HMDP Tracer

Animals in the primary tumor group underwent scintigraphic examinations on days 12, 30, and 48 after surgery. Animals in the recurrence group underwent scintigraphy on days 15 and 55 after intralesional curettage. For each paw, delayed images (10-min duration) were acquired 2 h after injection (30 MBq/animal).

^{99m}Tc-HMDP scans were analyzed at each time point using the TBR method.

Endpoint Histologic Analysis

At the endpoint of the imaging study, representative animals of both groups were sacrificed for histologic characterization of the tumors. The femora and tumor of each rat were removed and fixed at 4°C for 48 h in formol buffer (pH = 7.4). The femora were cut longitudinally or transversally. Decalcified femoral fragments were embedded in paraffin, and 5-μm sections were mounted on glass slides for routine hematoxylin-eosin-safranin staining.

RESULTS

Characterization of the 2 Experimental Tumor Models

Tumor volumes were followed for 50 d after primary implantation (Fig. 2A, left) and intralesional curettage (Fig. 2A, right). A tumor developed in all animals, becoming palpable from day 10 after primary implantation and day 8 after intralesional curettage.

The body weights of both groups of rats showed small increases over time.

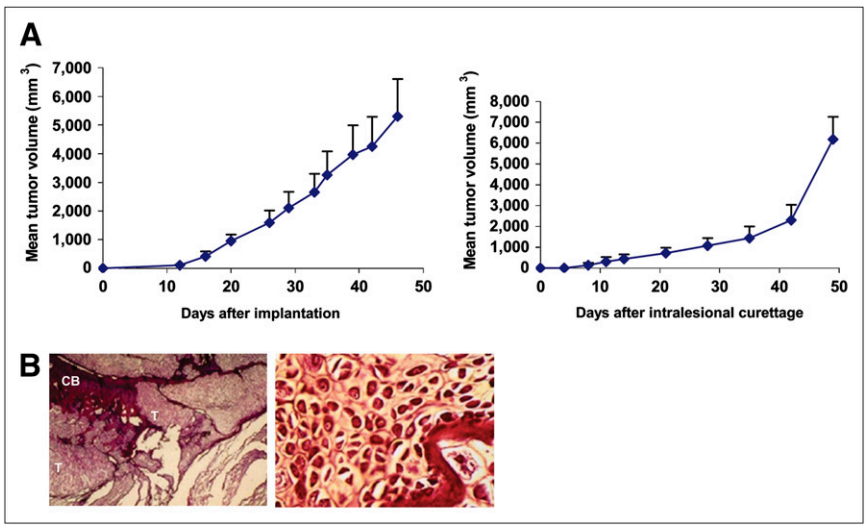

FIGURE 2. Characterization of SRC models. (A) Tumor volume growth curves for primary paratibial tumor model (left) and local recurrence tumor model (right); error bars represent SD. (B) Histomorphologic features of primary tumor model at study end showing replacement of cortical resorption by tumoral tissue (left) (×16). Hypercellularity and large irregular vesicular nuclei were also observed (right) (×400). CB = cortical bone; T = tumor.

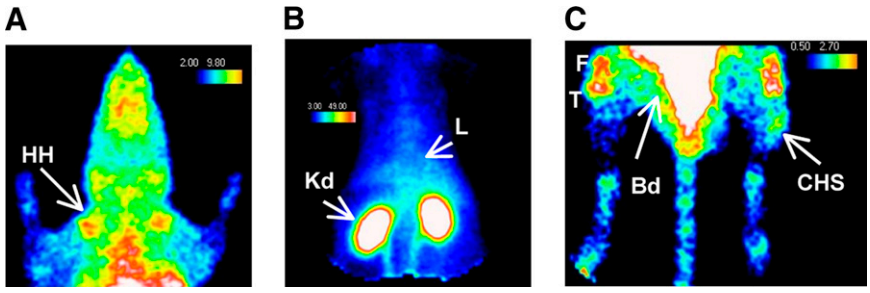

FIGURE 3. ^{99m}Tc-NTP 15-5 in vivo biodistribution in representative primary chondrosarcoma-bearing rat: (A) chest, (B) abdomen, and (C) posterior paws on day 4. Bd = bladder; CHS = chondrosarcoma; F = femoral condyle cartilage; HH = humeral head; Kd = kidney; L = liver; T = tibial plateau cartilage.

Histologic examination at the end of the study evidenced lobular, poorly vascularized chondroid tumoral tissue, with the lobules containing chondroid stroma and delimited by fine fibrous septa (Fig. 2B, left). Hypercellularity was also observed (Fig. 2B, right). At this later stage of disease, extensive invasion of bone and surrounding tissues was present, as well as central tumor necrosis.

Tolerance to Repeated Injection of ^{99m}Tc-NTP 15-5 and ^{99m}Tc-HMDP Radiotracers

Repeated injections of both tracers were well tolerated over 2 mo.

^{99m}Tc-NTP 15-5 Imaging of the Primary SRC Model

As shown in Figure 3 for a representative animal examined on day 4 after implantation, multiple sequential static acquisitions evidenced specific tracer accumulation in articular cartilage (i.e., the humeral head and the femorotibial joint, with the tibial plateau uptake clearly distinguished from the femoral condyle uptake), tracer accumulation at the site of tumor implantation, and nonspecific accumulation of tracer in liver and kidneys. Bone and muscle did not show any specific accumulation of tracer.

Visual inspection of ^{99m}Tc-NTP 15-5 scintigraphs at various time points after implantation (Fig. 4A) showed ^{99m}Tc-NTP 15-5 accumulation at sites of implantation on day 4 (for 8 animals of 12) and increasing radiotracer accumulation within the tumor-bearing paw as the tumor grew over time.

^{99m}Tc-NTP 15-5 accumulation was quantitatively assessed in the contralateral and tumor-bearing paws as a function of time after implantation.

No significant changes were seen in the contralateral cartilage uptake, as demonstrated by a mean TBR_C threshold of 2.03 ± 0.12 throughout the study (Fig. 4B, black bars).

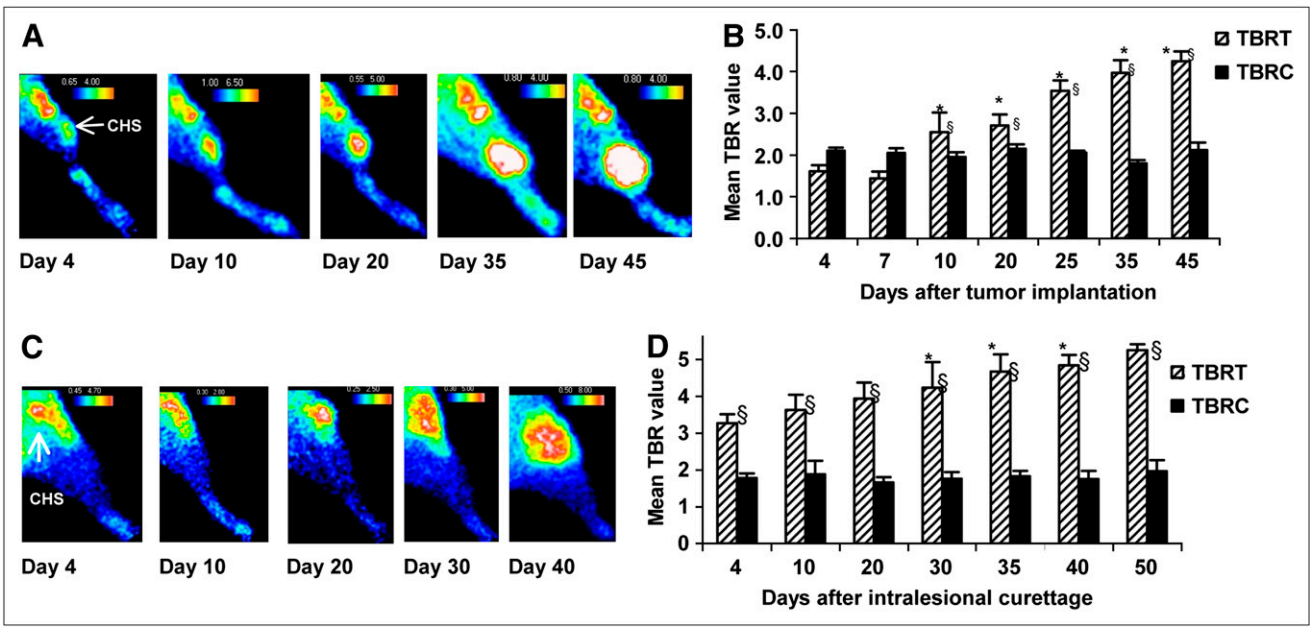

FIGURE 4. ^{99m}Tc-NTP 15-5 longitudinal in vivo examination of both models of SRC. (A) Scintigraphic images obtained for primary tumor model at various stages of study. Accumulation of radioactivity was clearly observed at site of implant by day 4 (arrow) (B) Quantitative analysis of ^{99m}Tc-NTP 15-5 accumulation in contralateral joint and primary tumor-bearing paw against time after implantation. (C) Scintigraphic images obtained for recurrent tumor model at various stages of study. (D) Quantitative analysis of ^{99m}Tc-NTP 15-5 accumulation in contralateral joint and recurrent tumor-bearing paw against time after curettage. Mean TBR + SD is presented at each time point. CHS = chondrosarcoma. *Statistically different from TBR_T threshold on day 4 ($P < 0.05$). §Statistically higher than TBR_C threshold ($P < 0.05$).

Considering tumoral uptake (Fig. 4B, hatched bars), the TBR_T threshold reference value was 1.6 ± 0.14 on day 4. As the tumors grew, TBR_T increased over time in the same animals: From day 10, ^{99m}Tc-NTP 15-5 scintigraphy showed that TBR_T was significantly increased ($P < 0.05$), compared with the day 4 TBR_T threshold reference. On day 45 (a stage of disease corresponding to a tumor volume of 5,302.8 ± 1,308 mm^3), the TBR_T was 4.25 ± 0.25. Tumor uptake was also compared with contralateral cartilage uptake: TBR_T was significantly higher ($P < 0.05$) than the TBR_C threshold from day 10 (2.55 ± 0.47 vs. 1.95 ± 0.11) and corresponded to a tumor volume of 217.5 ± 48.6 mm^3.

^{99m}Tc-NTP 15-5 distribution in primary chondrosarcoma was characterized through dynamic planar imaging. As shown by the time–activity curves in Figure 5, ^{99m}Tc-NTP 15-5 was rapidly taken up by SRC tissue, with radioactivity peaking 7 min after intravenous administration. A plateau was observed starting 15–20 min after injection and was maintained for at least 90 min. From the 15th minute after injection, TBR_T was 2.91 ± 0.58 over the whole 90-min acquisition. ^{99m}Tc-NTP 15-5 uptake in the tumor was higher than the femorotibial joint activity starting 30 min after injection (tumor-to-cartilage ratio, 1.43 ± 0.16 over the 30- to 90-min period). Interestingly, this ratio was higher at 60 min after injection, with a mean of 1.54 ± 0.17.

^{99m}Tc-NTP 15-5 Imaging of the Recurrent SRC Model

Visual inspection of ^{99m}Tc-NTP 15-5 scans at several time points showed an accumulation of radiotracer at sites of intralesional curettage starting on day 4 (6 animals of 9) and increasing over time with recurrence (Fig. 4C).

^{99m}Tc-NTP 15-5 accumulation was quantitatively assessed in the contralateral and tumor-bearing paws as a function of time after curettage. No significant changes were observed in the contralateral cartilage uptake, as shown by a mean TBR_C threshold of 1.80 ± 0.10 throughout the study (Fig. 4D, black bars).

Considering tumoral uptake (Fig. 4D, hatched bars), the TBR_T threshold reference was 3.27 ± 0.24 on day 4. As the tumors grew, TBR_T increased over time in the same animals. From day 30, ^{99m}Tc-NTP 15-5 scintigraphy showed that TBR_T increased significantly ($P < 0.05$), compared with the day 4 TBR_T threshold reference. On day 50, TBR_T was 5.25 ± 0.49 and corresponded to a tumor volume of 6,175.7 ± 1,083.0 mm^3.

Uptake at the site of curettage was also compared with that in the contralateral cartilage: TBR_T was significantly higher ($P < 0.05$) than the TBR_C threshold starting on day 4 (3.27 ± 0.24 vs. 1.8 ± 0.1) (Fig. 4D). At this stage of disease, tumor was not palpable or measurable.

Scintigraphic Imaging of Both Primary and Recurrent Chondrosarcoma Using ^{99m}Tc-HMDP Bone Radiotracer

For both groups, ^{99m}Tc-HMDP scans did not allow any positive imaging of either the primary tumor or local recurrent tumor, with TBRs of approximately 1 throughout the study (data not shown). At the later stage of study (day 48 for the primary model and day 55 for the recurrence model), an area of tracer accumulation in the diaphysis of the bone adjacent to the tumoral tissue was observed (Fig. 6).

DISCUSSION

Many prior results showed ^{99m}Tc-NTP 15-5 to be a good candidate SPECT tracer for the functional imaging of cartilage in nuclear medicine (*21–23*). The purpose of this experimental study was to assess the ability and usefulness of ^{99m}Tc-NTP 15-5 for detecting cartilage tumoral tissue in vivo and so to appraise the clinical and pathophysiologic validity of ^{9m}Tc-NTP 15-5 scintigraphy for in vivo chon-

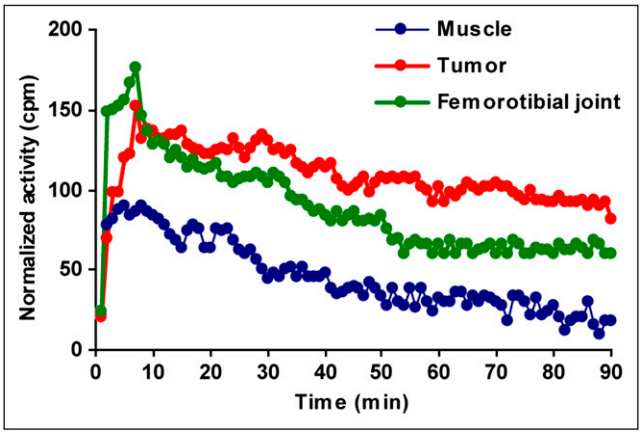

FIGURE 5. In vivo ^{99m}Tc-NTP 15-5 distribution in primary chondrosarcoma-bearing rats by dynamic planar imaging. Mean time–activity curves for uptake in femorotibial joint, muscle, and tumor are presented (for better legibility, error bars are not plotted).

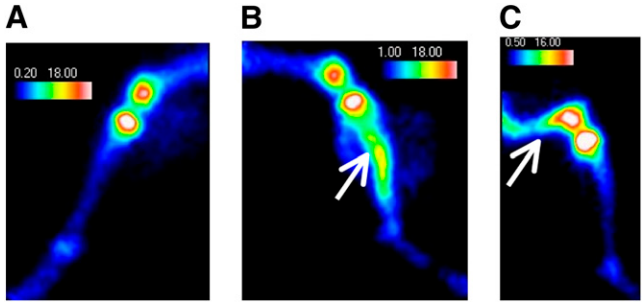

FIGURE 6. ^{99m}Tc-HMDP in vivo examination at later stage of study for both primary model and tumor recurrence model. Images are of same animal as that examined with ^{99m}Tc-NTP 15-5 and presented in Figure 4. Uptake was seen in bone diaphysis adjacent to tumoral tissue (tibia for primary model and femur for recurrent model [arrows]): (A) contralateral paw, (B) primary tumor model in paratibial location on day 48 after implantation, (C) recurrent tumor model in femoral condyle location on day 55 after curettage.

drosarcoma imaging. Our study used 2 preclinical approaches with the syngeneic SRC model: primary tumor paratibial location, and tumor local recurrence after intralesional curettage (*24,25*). We chose the SRC model because it has been extensively characterized, both histologically and biochemically. SRC is a well-differentiated malignant tumor. It features a characteristic lobulated form separated by thin vasculoconnective septa. As in other tumors, regressive processes are common, including areas of necrosis. The histologic and clinical behavior of SRC mimics human grade II disease, with local growth of the tumor, which invades and destroys host bone and produces metastases and ultimately the death of the rat (*27–30*). Large, aggregating proteoglycans have been described as a major component of the proteoglycan matrix of SRC (*27–29*). The high sulfate and carboxyl group content of their glycosaminoglycan moieties give proteoglycans of extracellular matrix strong negative charges that may interact with the positively charged quaternary ammonium moiety of the ^{99m}Tc-NTP 15-5 radiotracer. On the basis of our previous works on cartilage, we hypothesized that chondrosarcoma imaging with ^{99m}Tc-NTP 15-5 could result from the ionic interaction between the radiotracer and the negative charges of proteoglycans of extracellular matrix, which are highly concentrated in the tumor. Nevertheless, cellular binding cannot be excluded. Because the purpose of this in vivo study was to perform a sequential ^{99m}Tc-NTP 15-5 scintigraphic imaging study on animals with developing tumors, we did not have at our disposal tumor specimens for proteoglycan dosage (which required sacrifice of the animals). Such a study would therefore be of high interest and needs to be performed.

The ability of the ^{99m}Tc-NTP 15-5 radiotracer to image cartilaginous tumoral tissue was first investigated in the primary SRC model. Because of the paratibial location of the tumoral model, tracer accumulation was easily detected at the site of implantation by the first examination on day 4, and in more than 70% of the animals. Such early accumulation raised the question of whether the imaging pattern (and a TBR_T threshold reference of 1.6 ± 0.14) represented effective tumoral uptake or a surgery-induced inflammatory reaction. The question was also raised of whether ^{99m}Tc-NTP 15-5 imaging would be sufficiently sensitive to detect the in vivo proteoglycan content changes associated with early tumoral growth. We strongly believe in the tumoral-uptake hypothesis on the basis of the 2 following arguments: first, that no "clinical" sign of inflammation developed in the animals at the site of surgery (as assessed by measuring the 2 diameters of the paws), and second, that ^{99m}Tc-NTP 15-5 scintigraphy was previously shown to be highly sensitive for quantifying in vivo lower changes in proteoglycan content (*23*). Nevertheless, sequential imaging of sham-operated animals will be necessary for definitely ruling out the hypothesis of inflammation contribution. Considering that an especially useful application would be the diagnosis of local recurrence after surgery, we therefore assessed the relevance of ^{99m}Tc-NTP 15-5 imaging in the recurrent tumor model. Radiotracer accumulation was clearly observed at sites of curettage, starting on day 4 after surgery, with a high TBR_T. This finding could also be attributable to inflammation, residual tumor tissue at the site of surgery, or effective tumor recurrence.

Mean TBR_T was significantly higher in the recurrence model (range, 3.27–5.25) than in the primary model (range, 1.61–4.25), as is attributable to the location of the tumors. Given the femoral condyle location of the recurrent tumor, the ROI delineated over the tumor signal may have included a joint signal. There was a significantly enhanced signal intensity related to tumor occurrence in the joint.

For clinical application in patients with chondrosarcoma (located in the joint), comparison of uptake in the tumor and in the contralateral joint will be of particular importance and needs to be optimized. The kinetics of ^{99m}Tc-NTP 15-5 distribution in primary chondrosarcoma show that the ratio of tumor to femorotibial cartilage was better at 60 min after injection. Consequently, acquisition at 1 h after injection seems preferable.

Bone scintigraphy commonly used in clinical practice failed to detect changes in ^{99m}Tc-HMDP uptake throughout the study. At the advanced stage of disease and for both models, ^{99m}Tc-HMDP scans showed an area of tracer accumulation in the diaphysis attributable to the osteoblastic activity associated with the intraosseous extent of the tumor, as previously described in clinical situations (*31–33*).

In clinical practice, a wide range of nuclear medicine radiotracers can be used to characterize biologic phenotypes of chondrosarcomas (*31–41*). These include ^{99m}Tc-labeled biphosphonate (for the evaluation of bone involvement) and many tumor-seeking agents, such as ^{201}Tl, ^{99m}Tc-MIBI, ^{99m}Tc-tetrofosmin, ^{99m}Tc-DMSA(V), and more recently ^{18}F-FDG. All have been found useful in the initial diagnosis, grading, and evaluation of response to therapy of the high-grade tumors, but they have also shown limitations for imaging chondrosarcoma with low cellularity and low vascularity.

From our experimental results with the SRC model, we may hypothesize that ^{99m}Tc-NTP 15-5 scintigraphic imaging will provide suitable criteria for the evaluation of the tumoral pathology of cartilage in vivo.

CONCLUSION

These first results in experimental models of grade II chondrosarcoma bring forward data in favor of ^{99m}Tc-NTP 15-5 as a potential radiotracer of cartilage that could find use in orthopedic oncology. In the light of such encouraging preliminary results, the mechanism of binding to the tumor should be extensively characterized.

ACKNOWLEDGMENTS

This work was supported by the Institut National du Cancer ("Projet libre intercancéropôle CLARA/Grand Ouest," grant R07022NN) and by the Ligue Contre le Cancer, Comité Auvergne.

REFERENCES

1. World Health Organization. Cartilage tumors. In: Fletcher CDM, Unni KK, Mertens F, eds. *World Health Organization Classification of Tumors: Pathology and Genetics—Tumors of Soft Tissue and Bone.* Lyon, France: IARC Press; 2002:234–257.
2. Fiorenza F, Abudu A, Grimer RJ, et al. Risk factors for survival and local control in chondrosarcoma of bone. *J Bone Joint Surg Br.* 2002;84:93–99.
3. Lee FY, Mankin HJ, Frondren G, et al. Chondrosarcoma of bone: an assessment of outcome. *J Bone Joint Surg Am.* 1999;81:326–338.
4. Pritchard DJ, Lunke RJ, Taylor WF, Dahlin DC, Medley BE. Chondrosarcoma: a clinicopathological and statistical analysis. *Cancer.* 1980;45:149–157.
5. Donati D, El Ghoneimy A, Bertoni F, Di Bella C, Mercuri M. Surgical treatment and outcome of conventional pelvic chondrosarcoma. *J Bone Joint Surg Br.* 2005;87:1527–1530.
6. Gelderblom H, Hogendoorn PCW, Dijkstra SD, et al. The clinical approach towards chondrosarcoma. *Oncologist.* 2008;13:320–329.
7. Masciocchi C, Sparvoli L, Barile A. Diagnostic imaging of malignant cartilage tumors. *Eur J Radiol.* 1998;27(suppl 1):S86–S90.
8. Ollivier L, Vanel D, Leclere J. Imaging of chondrosarcomas. *Cancer Imaging.* 2003;4:36–38.
9. Evans HL, Ayala AG, Romsdahl MM. Prognostic factors in chondrosarcoma of bone: a clinicopathologic analysis with emphasis on histologic grading. *Cancer.* 1977;40:818–831.
10. Schajowicz F. *Histological Typing of Bone Tumors.* New York, NY: Springer-Verlag; 1993.
11. Aigner T, Muller S, Neureiter D, Illstrup DM, Kirchner T, Björnsson J. Prognostic relevance of cell biologic and biochemical features in conventional chondrosarcomas. *Cancer.* 2002;94:2273–2281.
12. Mankin HJ, Cantley KP, Lipiello L, Schiller AL, Campbell CJ. The biology of human chondrosarcoma I. Description of the cases, grading and biochemical analysis. *J Bone Joint Surg Am.* 1980;62:160–176.
13. Aigner T, Dertinger S, Vornehm SI, Dudhia J, Von der Mark K, Kirchner T. Phenotypic diversity of neoplastic chondrocytes and extracellular matrix gene expression in cartilaginous neoplasms. *Am J Pathol.* 1997;150:2133–2141.
14. Aigner T. Towards a new understanding and classification of chondrogenic neoplasias of the skeleton: biochemistry and cell biology of chondrosarcoma and its variants. *Virchows Arch.* 2002;441:219–230.
15. De Beuckeleer LH, De Schepper AM, Ramon F. Magnetic resonance imaging of cartilaginous tumors: is it useful or necessary? *Skeletal Radiol.* 1996;25:137–141.
16. Bovee JV, Hogendoorn CW. Cartilage-forming tumours of bone and soft tissue and their differential diagnosis. *Curr Diagn Pathol.* 2001;7:223–234.
17. Asghar K, Roth LJ. Distribution of hexamethonium and other quaternary ammonium compounds in cartilage. *J Pharmacol Exp Ther.* 1971;176:83–92.
18. Garrigue H, Maurizis JC, Madelmont JC, et al. Disposition and metabolism of acetylcholinesterase reactivators 2PAM-I, TMB4 and R665 in rats submitted to organophosphate poisoning. *Xenobiotica.* 1991;21:583–595.
19. Madelmont JC, Giraud I, Nicolas C, et al., inventors. Cyclopharma Laboratoires, assignee. Novel quaternary ammonium derivatives, method for preparing same and pharmaceutical use. International patent PCT WO 01/00621 A1. January 2001.
20. Nicolas C, Borel M, Maurizis JC, et al. Synthesis of N-quaternary ammonium [^{3}H] and [^{99m}Tc] polyazamacrocycles, potential radiotracers for cartilage imaging. *J Labelled Comp Radiopharm.* 2000;43:585–594.
21. Maurizis JC, Rapp M, Nicolas C, et al. Disposition in rats of N-pyridinium-propyl-cyclam, N-triethylammonium-propyl-cyclam, and N-[triethylammonium]-3-propyl-[15]ane-N5, potential cartilage imaging agents. *Drug Metab Dispos.* 2000;28:418–422.
22. Ollier M, Maurizis JC, Nicolas C, et al. Joint scintigraphy in rabbits with ^{99m}Tc-N-[3-(triethylammonio)propyl]-15ane-N5, a new radiodiagnostic agent for articular cartilage imaging. *J Nucl Med.* 2001;42:141–145.
23. Miot-Noirault E, Vidal A, Pastoureau P, et al. Early detection and monitoring of cartilage alteration in the experimental meniscectomised guinea pig model of osteoarthritis by ^{99m}Tc-NTP 15-5 scintigraphy. *Eur J Nucl Med Mol Imaging.* 2007;34:1280–1290.
24. Gouin F, Ory B, Redini F, Heymann D. Zoledronic acid slows down rat primary chondrosarcoma development, recurrent tumor progression after intralesional curettage and increases overall survival. *Int J Cancer.* 2006;119:980–984.
25. Grimaud E, Damiens C, Rousselle AV, Passuti N, Heymann D, Gouin F. Bone remodelling and tumor grade modifications induced by interactions between bone and Swarm rat chondrosarcoma. *Histol Histopathol.* 2002;17:1103–1111.
26. *Guide for the Care and Use of Laboratory Animals.* Washington, DC: National Academy Press; 1996.
27. Hascall GK. Ultrastructure of the chondrocytes and extracellular matrix of the Swarm rat chondrosarcoma. *Anat Rec.* 1980;198:135–146.
28. Breitkreutz D, Diaz de Leon L, Paglia L, Gay S, Swarm RL, Stern R. Histological and biochemical studies of a transplantable rat chondrosarcoma. *Cancer Res.* 1979;39:5093–5100.
29. Oegema TR Jr, Hascall VC, Dzwiewiatkowski DD. Isolation and characterization of proteoglycans from the Swarm rat chondrosarcoma. *J Biol Chem.* 1975;250:6151–6159.
30. Kenan S, Steiner GC. Experimental transplantation of the Swarm rat chondrosarcoma into bone: radiological and pathological studies. *J Orthop Res.* 1991;9:445–451.
31. Hicks RJ. Nuclear medicine techniques provide unique physiologic characterization of suspected and known soft tissue and bone sarcomas. *Acta Orthop Scand Suppl.* 1997;273:25–36.
32. Arsos G, Venizelos I, Karatzas N, Koukoulidis A, Karakatsanis C. Low-grade chondrosarcomas: a difficult target for radionuclide imaging—case report and review of the literature. *Eur J Radiol.* 2002;43:66–72.
33. Hendel HW, Daugaard S, Kjaer A. Utility of planar bone scintigraphy to distinguish benign osteochondromas from malignant chondrosarcomas. *Clin Nucl Med.* 2002;27:622–624.
34. Kobayashi H, Kotoura Y, Hosono M, et al. Diagnostic value of Tc-99m (V) DMSA for chondrogenic tumors with positive Tc-99m HMDP uptake on bone scintigraphy. *Clin Nucl Med.* 1995;20:361–364.
35. Söderlund V, Jonsson C, Bauer HC, Brosjö O, Jacobsson H. Comparison of technetium-99m-MIBI and technetium-99m-tetrofosmin uptake by musculoskeletal sarcomas. *J Nucl Med.* 1997;38:682–686.
36. Büyükdereli G, Sargin O, Ozbarlas S. Tc-99m tetrofosmin imaging in chondrosarcoma. *Clin Nucl Med.* 2000;1:64–65.
37. Choong PF, Kunisada T, Slavin J, Schlicht S, Hicks R. The role of thallium-201 and pentavalent dimercaptosuccinic acid for staging cartilaginous tumors. *Int Semin Surg Oncol.* 2004;8:10.
38. Higuchi T, Taki J, Sumiya H, et al. Characterization of cartilaginous tumors with ^{201}Tl scintigraphy. *Ann Nucl Med.* 2005;19:95–99.
39. Lee FY, Yu J, Chang SS, Fawwaz R, Parisien MV. Diagnostic value and limitations of fluorine-18 fluorodeoxyglucose positron emission tomography for cartilaginous tumors of bone. *J Bone Surg Am.* 2004;86-A:2677–2685.
40. Feldman F, Van Heertum R, Saxena C, Parisien M. ^{18}FDG-PET applications for cartilage neoplasms. *Skeletal Radiol.* 2005;34:367–374.
41. Brenner W, Conrad EU, Eary JF. FDG PET imaging for grading and prediction of outcome in chondrosarcoma patients. *Eur J Nucl Med Mol Imaging.* 2004;31:189–195.